

# SATELLITE BASED T-S DIAGRAMS: A PROSPECTIVE TOOL TO TRACE OCEAN WATER MASSES

Roberto Sabia<sup>(1)</sup>, Marlene Klockmann<sup>(1)</sup>, Craig Donlon<sup>(2)</sup>, Diego Fernández-Prieto<sup>(1)</sup>, Marco Talone<sup>(3)</sup>, Joaquim Ballabrera<sup>(3)</sup>

<sup>(1)</sup> ESA, ESRIN, Via Galileo Galilei, 00044 Frascati, Italy, Email: roberto.sabia@esa.int

<sup>(2)</sup> ESA, ESTEC, Postbus 299, 2200 AG Noordwijk, The Netherlands, Email: craig.donlon@esa.int

<sup>(3)</sup> SMOS-BEC, Passeig Marítim de la Barceloneta, 37-49, 08003 Barcelona, Spain, Email: joaquim@imc.csic.es

## ABSTRACT

Temperature-Salinity (T-S) diagrams are derived from SMOS and Aquarius Sea Surface Salinity (SSS) and OSTIA Sea Surface Temperature (SST) in order to characterize the (co-)variability of SST and SSS in four regions of the North Atlantic. Comparison with in-situ data from Argo floats is used to assess the new information that the satellite data provide with respect to Argo and gain further insights into the processes that govern the near-surface stratification. The surface T-S signatures as seen by the satellites and Argo show similar patterns, with SMOS detecting fresher SSS values, as expected, and OSTIA showing a tendency to be warmer than Argo. Part of this fresher misfit can be attributed to precipitation, whilst the effect of other parameters are being assessed. On-going efforts are devoted to link these signatures with the water masses formation.

## 1. INTRODUCTION

Temperature-Salinity (T-S) diagrams emphasize the relationship between observations of temperature and salinity and connect them to the density of the water body. Typically they are derived from in-situ vertical profiles such as CTD casts. Assuming that T and S are conservative properties, i.e. that away from the ocean surface they can only be modified by mixing, specific T-S curves can be used to identify water masses in regions other than their formation area and to trace their movements. Processes that modify water characteristics are precipitation (P) and evaporation (E), solar heating or surface cooling, freezing or melting of sea-ice, river run-off and horizontal/vertical advection and mixing. An overview of the major water masses is given in [1]. Until now, water mass classification has been dependent on in-situ measurements which have poor temporal and spatial coverage. Typically the upper meters of the profiles are not taken into account, since measurements are less reliable there. With the advent of SMOS [2] and Aquarius/SAC-D [3] missions, satellite observations of Sea Surface Salinity (SSS) have become available with global coverage and higher temporal frequency. Together with spaceborne Sea Surface Temperature (SST) measurements, it is now possible for the first time to observe the surface T-S signature on a global scale and to assess also its temporal (co-) variability.

This study presents satellite-based, horizontal T-S diagrams as a means to assess the temporal evolution of covariability of SST and SSS. The main objectives are (1) to dynamically characterize the SSS and SST in relation to existing climatology and in-situ data, improving our understanding of their distribution and variability and (2) to understand the unique information that SMOS and Aquarius SSS data are providing with respect to climatology or in-situ measurements.

The T-S diagrams are produced from SMOS and Aquarius Optimally-Interpolated (OI) SSS (Level 3 products, L3) and the Operational Sea Surface Temperature and Sea Ice Analysis (OSTIA) SST [4]. The satellite-based T-S diagrams are compared with ARGO based T-S diagrams which use SST and SSS from Near Real Time ARIVO monthly fields (in the following referred to as *Argo NRT*) [5]. SST and SSS from the World Ocean Atlas 2009 (WOA09, [6,7]) are used for a comparison with climatology.

A fresh bias of SMOS with respect to Argo data was expected, as it was found in previous studies [see e.g. 8], where it was highlighted that the distribution of (SMOS SSS – Argo SSS) is shifted towards negative values. Such fresh misfit may be evidence for an ear-surface stratification during and shortly after rain events, and rain lenses would be more likely to be detected by satellite measurements than by Argo floats (which often limit their measurement to about 5m below the surface).

Another big challenge is, moreover, to distinguish between the new information that the satellites are providing with respect to Argo data and to the WOA09 climatology and the biases and errors currently experienced by the satellites (due to e.g. the roughness models applied in the SSS retrieval at L-band or external noise sources such as Galactic noise, Sun glint or RFI, [9]).

## 2. METHODS

### 2.1. Study area

The study area is currently set in the North Atlantic from 55 N to 20 S. Within this area, four sub regions have been defined (see Fig. 1), as representative of four different regimes: 1) large SST and SSS gradients over the Gulf Stream front with the impact of overpassing synoptic weather systems; 2) the subtropical regime

with high SSS, strong evaporation, very small gradients of SSS and SST over the salinity maximum; 3) small SST range, as present in the freshwater plumes of two large rivers, the Amazon and the Orinoco, with consequently large gradients and high temporal variability in SSS; and 4) the tropical regime of the equatorial Atlantic with strong precipitation resulting from atmospheric deep convection.

## 2.2. T-S diagrams

For each sub region, SST is plotted against SSS. This has been done for monthly and seasonally-averaged data. Within this paper, seasonal averages are shown if not otherwise noted. Sea surface density ( $\sigma_s = \rho - 1000 \text{ kg/m}^3$ ) is calculated using the equation of state TEOS10 [10]. Therefore temperature and salinity have been converted to conservative temperature (given in

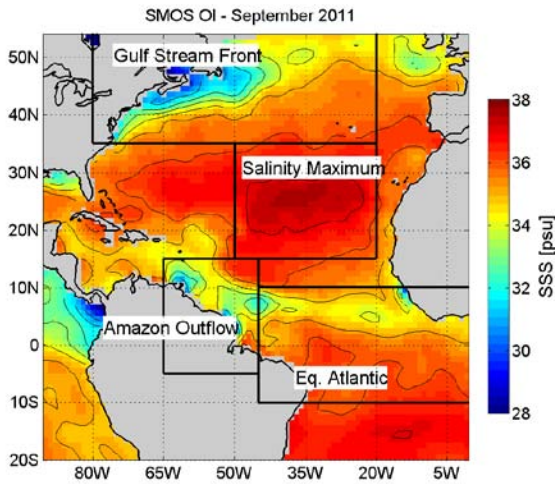


Figure 1. SMOS SSS in September 2011; the four sub regions are outlined by black rectangles

$^{\circ}\text{C}$ ) and absolute salinity (given in g/kg). Otherwise, psu (practical salinity unit) according to the Practical Salinity Scale (PSS78) are used, if not further specified. For more details on the T-S diagrams see also [11].

## 2.3. Comparison with Argo data

For the comparisons with Argo NRT and WOA09, the calculation of the differences between OSTIA SST and Argo NRT/WOA 09 SST and between SMOS/Aquarius SSS and Argo NRT/WOA09 SSS, respectively, are performed and  $d\text{SST}$  against  $d\text{SSS}$  are plot.

From these, a combined mismatch is calculated, defining a mismatch radius and a mismatch angle  $\varphi$  as follows:

$$r = \sqrt{d\text{SST}^2 + d\text{SSS}^2} \quad (1)$$

$$\varphi = \arctan(d\text{SST} / d\text{SSS}) \quad (2)$$

Further details on the mismatch calculation can be found in [12].

## 3. DATA

ESA's SMOS mission was launched in November 2009 and is in its operational phase since May 2010. Its Microwave Imaging Radiometer using Aperture Synthesis (MIRAS) measures brightness temperature at L-Band from multiple incidence angles. SSS is then retrieved with an iterative inversion scheme [13]. Monthly SMOS L3 OI product are used, with a spatial resolution of  $1^{\circ}$  by  $1^{\circ}$  derived from ascending passes obtained with v550 of the L2OS processor. The third roughness model, which improved the salinity retrieval under high wind seed conditions [14], is used.

Aquarius/SAC-D is a combined active/passive US/Argentinean mission launched in June 2011 and it is operational since December 2011. A key capability of Aquarius lies in its L-band scatterometer which provides collocated roughness information needed as auxiliary parameter for a proper SSS retrieval [15]. Aquarius v2.0 L3 SSS smoothed monthly fields with a spatial resolution of  $1^{\circ}$  by  $1^{\circ}$  are used according to [16]. The OSTIA data set provides daily foundation temperature fields derived from the satellites of the Group of High Resolution SST (GHRSSST) project, merged with in-situ observations and optimally interpolated to a grid with  $1/20^{\circ}$  resolution [4]. Daily fields have been averaged to a monthly product with a  $1^{\circ}$  by  $1^{\circ}$  resolution.

For the Argo NRT fields the Near Real Time Argo profiles provided by Coriolis are quality checked and interpolated onto a regular grid in combination with other local arrays (mooring and CTD data) using the In Situ Analysis System (ISAS, [17]). Monthly fields are provided with a  $0.25^{\circ}$  by  $0.25^{\circ}$  resolution at the equator. Again, the fields have been averaged to a  $1^{\circ}$  by  $1^{\circ}$  grid.

The WOA 09 data set provides a climatology of ocean temperature and salinity on a  $1^{\circ}$  by  $1^{\circ}$  grid composed of the objectively-analysed in-situ data available in the World Ocean Database from 1955 to 2006.

The time period of the study is currently limited to 2011, since the Argo NRT product has only recently been reprocessed and updated to 2012. Therefore the entire year of 2011 of SMOS and five months (August to December 2011) of Aquarius data have been used.

## 4. RESULTS

### 4.1. Co-variability of SST and SSS

Figure 2 shows some examples of the analysed T-S variability in the various regions and seasons. Over the Amazon/Orinoco outflow the SST range is very small with 25 to  $28^{\circ}\text{C}$  throughout the year. OSTIA SST is somewhat warmer than Argo SST in summer. SSS ranges from 37 to 33 (31) psu in winter (summer) with

outliers as fresh as 22 psu. SMOS tends to be a bit fresher but does not show the very fresh outliers as Argo NRT. In summer, there are more points with SSS fresher than 34 psu. This corresponds well with the seasonal cycle of the river discharge of the Amazon and Orinoco. The discharge is maximum in May/June (July/August) for the Amazon (Orinoco) and minimum in October/November (February March) for the Amazon (Orinoco). The river discharge data is taken from [18]. In the equatorial Atlantic the T-S signature is more complex with a SST maximum of  $\sim 29/30^\circ\text{C}$  which is at the same time a minimum in SSS at 34 psu. The maximum SSS is at 37 psu with SST around  $28^\circ\text{C}$ . SST shows a minimum at  $25^\circ\text{C}$  with SSS between 35 and 36 psu. In summer there is no such clear min/max structure, the ranges are unchanged though. Over the Salinity maximum the T-S signature shows very little scatter. The SST range is larger in winter (17 to  $27^\circ\text{C}$ ) than in summer (22 to  $29^\circ\text{C}$ ). The SSS maximum is located at 38 psu. SMOS appears up to 1 psu fresher.

summer (JJA, below) lower right) of 2011.

Over the Gulf Stream front less data are available in winter (due to quality flagging). SST ranges from  $2.5$  to  $20^\circ\text{C}$  and SSS from 32 to 36.5 psu, where colder SST is connected with fresher SSS. In summer, SST is shifted towards warmer temperatures with a range from 12 to  $28^\circ\text{C}$ . Most points have a salinity between 34.4 and 37. There are scattered SSS points between 30 and 34 psu, observed in both Argo NRT and SMOS. SMOS tends again to be fresher. Over the Amazon/Orinoco outflow and the equatorial Atlantic the  $\text{SS}\sigma$  ranges between 21 and  $24\text{ kg/m}^3$  or is even smaller in case of the Amazon/Orinoco outflow in summer. Denser water with  $\text{SS}\sigma > 24\text{ kg/m}^3$  is present at the Salinity maximum and the Gulf Stream front. The densest water is found during the winter months at the Gulf Stream front exceeding  $27\text{ kg/m}^3$ .

#### 4.2. Comparison with Argo NRT

Figure 3 shows an example of the relative mismatch of the satellite and Argo data in the various regions and seasons. The Amazon/Orinoco outflow shows a low accuracy with respect to Argo NRT (a standard deviation of 1.38 in winter and 2.14 in summer) but the bias is very close to zero. The performance is best over the salinity maximum area. Here the accuracy is 0.14 in winter and 0.15 in summer. A reason for the good performance is surely the distance from land and the warm temperatures throughout the years. In winter there is a small bias of  $-0.13$  psu while in summer it is  $-0.32$  psu. The Gulf Stream front and the Equatorial Atlantic show a similar performance with a bias between  $-0.25$  and  $-0.41$  psu, while the accuracy lies between 0.27 and 0.35. In comparison with WOA09 (not shown), especially the SST bias is remarkably reduced.

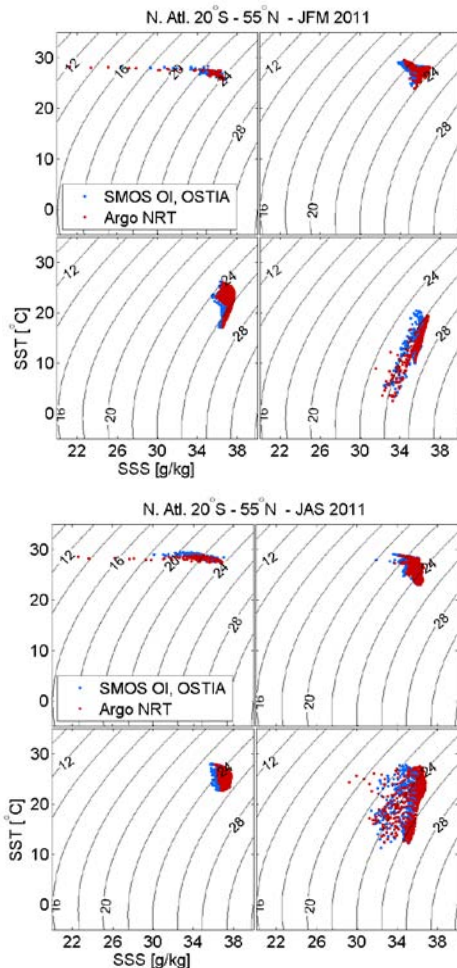
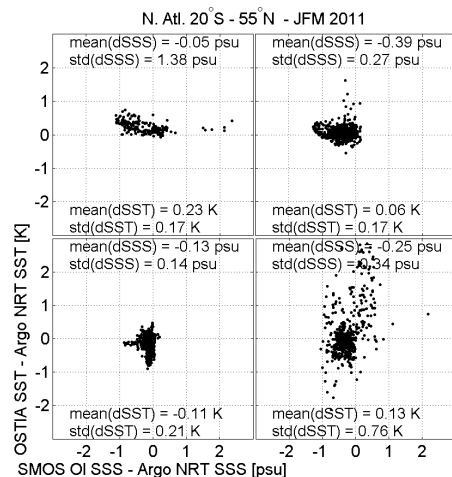


Figure 2. Seasonal averages of T-S diagrams comparing satellite data (blue dots) and Argo NRT data (red dots) in the four sub regions: Amazon/Orinoco (resp. upper left), eq. Atlantic (resp. upper right), Salinity maximum (resp. lower left), Gulf Stream front (resp. lower right) during winter (JFM, above) and



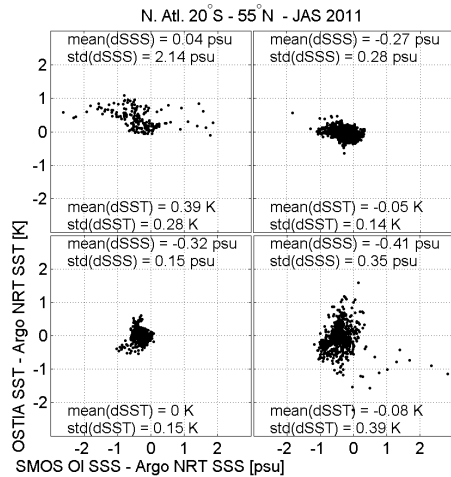


Figure 3. As Fig. 2 but for the seasonal averages of SST differences ( $dSST$ ) vs. SSS differences ( $dSSS$ ). Bias and accuracy of the satellite measurements with respect to Argo NRT are noted on the top ( $dSSS$ ) and bottom ( $dSST$ ) of the respective panels.

### 4.3. Geographical mismatch

In this section it will be analysed the differences between SMOS and Argo NRT in further detail. As a starting point, it should be noted that the satellites are measuring salinity at 1 cm depth while the Argo floats stop to measure near 5m depth, i.e. some differences might be induced by near-surface stratification.

Fig. 4 shows the classification of the combined mismatch using Eq. (1) and (2). Four classes are distinguished: overestimation of SST and SSS by the satellites with respect to Argo NRT (blue), underestimation of SST and SSS (yellow), overestimation of SST and underestimation of SSS (cyan) and underestimation of SST with overestimation of SSS (red). White indicates a mismatch radius smaller than 0.5 and light green marks points that have a large mismatch radius which is primarily induced by SST.

Fig. 5 shows an example for the distribution of quadrants for August 2011. Superimposed is the monthly mean precipitation. There is a good spatial agreement between areas of large negative  $dSSS$  (marked cyan and yellow) and areas where  $P$  exceeds 3 mm/day on a monthly average, specially over the Gulf Stream and off the African coast around 10°N. There are however, also areas where SMOS shows a fresher signal and the monthly average precipitation is below 3mm/day, e.g. in the very north east Atlantic and off the Northwest African coast.

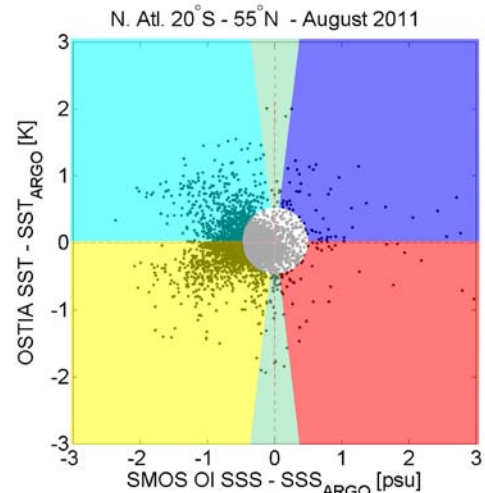
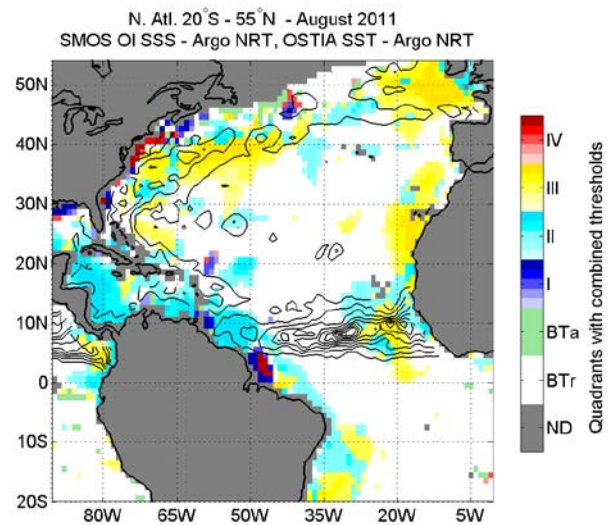


Figure 4. Classification of the mismatch into four different quadrants

The mismatch distribution using Aquarius SSS in Fig. 5 (lower panel) does not show this agreement. There are more points with mismatches below 0.5 and Aquarius SSS tends to be higher than Argo NRT SSS. Similar mismatch patterns of SMOS and Aquarius are mostly located in the region of the Amazon/Orinoco outflow, where  $P$  is low and the mismatch is therefore most probably not dominated by precipitation.



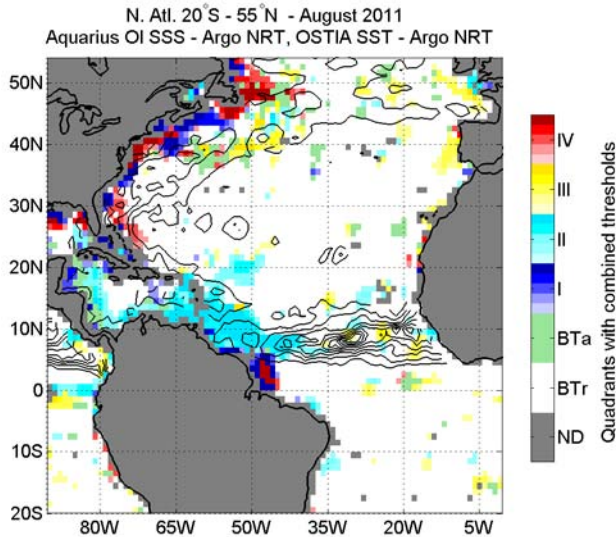


Figure 5. Quadrants of combined mismatch of  $dSST$  and  $dSSS$  for  $SST_{OSTIA} - SST_{Argo}$  with  $SSS_{SMOS} - SSS_{Argo}$  (above) and  $SSS_{Aquarius} - SSS_{Argo}$  (below), respectively.

Contours of CMORPH precipitation overlaid. The contour interval is 3 mm/day, starting from 3 mm/day. Colour intensity reflects the magnitude of the mismatch radius, ranging from 0.5 (light) to 1.5 (dark) in intervals of 0.2. ND: No data, BTr: points that are below a mismatch radius of 0.5, BTa: points within the angle segments marked green in Fig.4.

Overall Aquarius seems less sensitive to rain, as also mismatch cloud is centred around zero, while for SMOS it is shifted towards negative  $dSSS$ . Note that SMOS SSS shows the same pattern regardless of using the full year 2011 or only the months August to December 2011 (not shown).

## 5. CONCLUSIONS

The present study assessed the temporal variability of the T-S signature in different regimes of the North Atlantic and compared satellite derived SSS and SST with in-situ SSS and SST obtained from Argo floats. The surface T-S signature is determined by interaction with the atmosphere and is a link to the observation of water masses.

Two major challenges are envisaged: (1) to differentiate between the new information that the satellites are providing with respect to climatology/in-situ data and possible measurement/retrieval errors and (2) to understand which part of the surface signal is actually contributing to water mass formation, i.e. at which SSS and SST are specific density classes formed.

In the present study, the focus was oriented to the first challenge by relating  $dSSS$  and  $dSST$  to precipitation. SMOS showed some evident overlapping with some precipitation areas, but also a fresh bias in areas with little to no precipitation (over the salinity maximum), which suggests that only part of the fresher signal can be explained by precipitation. Some of the large

mismatch near the continents may be due to land contamination which has been reduced but is still present in the reprocessed SMOS data. On-going work is analysing other parameters influence (such as wind speed and surface density fluxes) on the retrieval and/or the near surface stratification.

Some efforts are already being dedicated to address the second challenge, using the T-S diagrams to identify the SSS and SST ranges that contribute to water mass formation and to better understand the link between the surface and deeper layers. Once longer time series of SSS become available this may become a tool to identify trends or shifts in the water mass formation.

## 6. ACKNOWLEDGEMENTS

The authors thank Fabienne Gaillard who kindly provided the Argo NRT product. The SMOS L3 OI product is produced and provided by the SMOS Barcelona Expert Center. The Aquarius data is distributed by PO.DAAC. This study has been conducted using MyOcean products.

## 7. REFERENCES

- Emery, W. J. (2003). *Water Types and Water Masses, Ocean Circulation*, Elsevier science, pp 1556-1567.
- Font, J., Camps, A., Borges, A., Martín-Neira, M., Boutin, J., Reul, N., Kerr, Y.H., Hahne, A. & Mecklenburg, S. (2010). SMOS: The challenging sea surface salinity measurement from space. *Proceedings of the IEEE*, **98**, 649-665.
- Lagerloef, G. (2012) Satellite mission monitors ocean surface salinity. *Eos Trans. AGU*, **93**(25), 233-234
- Donlon, C.J., Martin, M., Stark, J.D., Roberts-Jones, J., Fiedler, E. & Wimmer, W. (2011). The Operational Sea Surface Temperature and Sea Ice analysis (OSTIA). *Remote Sensing of the Environment*, **116**, 140-158.
- Gaillard, F., Autret, E., Thierry, V., Galaup, P., Coatanoan, C. & Loubrieu, T. (2009). Quality control of large Argo data sets. *Journal of Atmospheric and Ocean Technology*, **26**(2), 337-351.
- Locarnini, R.A., Mishonov, A.V., Antonov, J.I., Boyer, T.P., Garcia, H.E., Baranova, O.K., Zweng, M.M. & Johnson, D.R. (2010). *World Ocean Atlas 2009, Volume 1: Temperature*. S. Levitus, Ed. NOAA Atlas NESDIS 68, (U.S. Government Printing Office, Washington, D.C.), 184 pp.
- Antonov, J.I., Seidov, D., Boyer, T.P., Locarnini, R.A., Mishonov, A.V., Garcia, H.E., Baranova, O.K., Zweng, M.M. & Johnson, D.R. (2010). *World Ocean Atlas 2009, Volume 2: Salinity*. S. Levitus, Ed. NOAA Atlas NESDIS 69, (U.S. Government Printing Office, Washington, D.C.),

184 pp.

8. Boutin, J., Martin, N., Reverdin, G., Yin, X. & Gaillard, F. (2013). Sea surface freshening inferred from SMOS and ARGO salinity: impact of rain. *Ocean Science*, **9**, 183-192.
9. Font, J., Boutin, J., Reul, N., Spurgeon, P., Ballabrera, J., Chuprin, A., Gabarró, C., Gourrion, J., Guimbard, S., Hénocq, C., Lavender, S., Martin, N., Martínez, J., McCulloch, M., Meirold-Mautner, I., Mugerin, C., Petitcolin, F., Portabella, M., Sabia, R., Talone, M., Tenerelli, J., Turiel, A., Vergely, J.-L., Waldteufel, P., Yin, X., Zine, S. & Delwart, S. (2013). SMOS first data analysis for sea surface salinity determination. *International Journal of Remote Sensing*, **34**( 9-10), 3654-3670.
10. McDougall, T.J. & Barker, P.M. (2011). *Getting started with TEOS-10 and the Gibbs Seawater (GSW) Oceanographic Toolbox*, (SCOR/IAPSO WG127), 28 pp.
11. Sabia, R., Ballabrera, J., Lagerloef, G., Bayler, E., Talone, M., Chao, Y., Donlon, C., Fernández-Prieto, D. & Font, J. (2012). Derivation of an Experimental Satellite-based T-S Diagram. In Proceedings of IGARSS '12, Munich, Germany, pp. 5760-5763.
12. Klockmann, M., R. Sabia, D. Fernandez-Prieto, C. Donlon, M. Talone, J. Font. (2013), Satellite-based TS Diagrams derived from SMOS, Aquarius and OSTIA data, 33rd EARSeL Symposium "Towards Horizon 2020: Earth Observation and Social Perspectives", 3-6 June 2013 - Matera, Italy.
13. Zine, S., Boutin, J., Font, J., Reul, N., Waldteufel, P., Gabarró, C., Tenerelli, J., Petitcolin, F., Vergely, J.L., Talone, M. & Delwart, S. (2008). Overview of the SMOS Sea Surface Salinity Prototype Processor. *IEEE Trans. Geosc. Remote Sens*, **46** (3), 621-645.
14. Guimbard, S., Gourrion, J., Portabella, M., Turiel, A., Gabarro, C. & Font, J. (2012). SMOS Semi-Empirical Ocean Forward Model Adjustment. *IEEE Transactions*, **55**(5), 1676 – 1687.
15. Le Vine, D.M., Lagerloef, G.S.E. & Torrusio, S.E. (2010). Aquarius and Remote Sensing of Sea Surface Salinity from Space. *Proceedings of the IEEE*, **98**(5), 688-703.
16. Lilly, J.M. & Lagerloef, G.S. (2008). *Aquarius Level 3 processing algorithm theoretical basis document: Version 0.9*. (Aquarius Ground Segment, Goddard Space Flight Center) 14 pp.
17. Gaillard, F, 2012. *ISAS-Tool Version 6: Method and Configuration, SO-ARGO report*, 45 pp
18. Dai, A., Qian, T., Trenberth, K.E. & Milliman, J.D. (2009). Changes in continental freshwater discharge from 1948-2004. *Journal of Climate*, **22**, 2773-2791.